Soft colloids driven and sheared by traveling wave fields

M. Rex, H. Löwen, and C. N. Likos
Institut für Theoretische Physik II, Heinrich-Heine-Universität Düsseldorf, Universitätsstraße 1, 40225 Düsseldorf, Germany
(Received 23 December 2004; revised manuscript received 4 April 2005; published 12 August 2005)

We study the dynamics of soft colloids interacting via a Gaussian pair potential in an external moving potential which is periodic in the spatial coordinate of the direction of motion. Both dynamical density functional theory and Brownian dynamics computer simulations are used to predict the steady-state density profiles. Two different situations are investigated: the first corresponds to a light wave that travels with a constant velocity v through the quiescent solvent containing the colloidal suspension. The second setup consists of two parallel repulsive walls with a periodic topographical substructure. One of the walls is at rest relative to the solvent while the other is in motion, inducing a shearing of the suspension. In the first case, we find that the amplitude of the steady-state density behaves nonmonotonically with the traveling speed v of the wave if the shape of the wave contains an edge: for increasing v, it first grows and then decreases. In the second setup we show that a strongly confined suspension induces a shear resistance which is a nonmonotonic function of the wall velocity. These effects are verifiable in real-space experiments on colloidal suspensions exposed to external laser-optical fields. In both situations, the dynamical density functional theory is in good agreement with the Brownian dynamics simulation data.

DOI: 10.1103/PhysRevE.72.021404 PACS number(s): 82.70.Dd, 61.20.Ja, 05.40.Jc

I. INTRODUCTION

Colloidal particles dispersed in a solvent can be manipulated easily by external fields, which bring them into nonequilibrium situations in a controlled way [1,2]. The simplest case for an external field corresponds to an external force acting on the colloidal particles [3]. Examples include gravity leading to sedimentation, an electric field acting on charged particles, or a laser-optical field, which provides an external potential to the particles due to their dielectric contrast with the solvent [4,5]. In the latter case, crossed laser beams constitute a static sinusoidal external potential, which is periodic in one spatial coordinate [6]. This leads to a laser-induced freezing transition of the colloidal particles and a reentrant melting for increasing amplitude of the external field [7].

While the equilibrium behavior of static (i.e., *time-independent*) external potentials is well understood by now, nonequilibrium situations as induced by, e.g., a *time-dependent* external field are much less investigated. Since equilibrium situations of inhomogeneous liquids and solids can be well described within the classical density functional theory of freezing [8,9], it is tempting to transfer this approach to dynamical situations [10]. In fact, recent work has shown that classical density functional theory can indeed be applied to time-varying confining external potentials even if the time scale of the variation is comparable to the Brownian time of the colloidal particles. This holds both for one-component systems [11,12] and for binary phase-separating mixtures, for which the demixing dynamics has been recently studied by Archer [13] using the dynamical density functional formalism. Another application of dynamical density functional theory pertains to the structural relaxation near the kinetic glass transition [14]. On a more rigorous level, it has been shown recently that a dynamical density functional does exist [15]. A tractable density functional within the mean-field approximation is justified for soft interparticle interactions [16] as described by, e.g., an effective Gaussian pair potential [17], which is realized for polymer coils [18] or dendrimers [19].

In this paper, we study another situation of a time-dependent external potential: namely, that of a traveling wave. Then the potential V_{ext} depends only on one coordinate z-vt where z is one spatial coordinate, t is time, and v is the traveling speed. In particular, we consider situations where $V_{\text{ext}}(z\text{-}vt)$ is a periodic function in z-vt. The traveling wave setup is motivated by recent experiments of Tanaka and coworkers [20]. They apply crossed laser beams to a colloidal suspension, resulting in a sinusoidal wave field which travels through the suspension with a constant velocity. The periodicity length of the external potential is of the order of the mean interparticle spacing. The impact of such a wave field on the steady state of the colloids has not been theoretically addressed before. In this paper, we use dynamical mean-field density functional theory and Brownian dynamics computer simulations to reveal the impact of a traveling wave field on colloidal particles that interact by means of a Gaussian pair potential. As a result, we predict that the steady-state colloidal density profiles induced by the traveling wave exhibit an unusual behavior: the amplitude of the density peak in the valleys of the periodic external potential behaves nonmonotonically with increasing traveling speed v. Hence, particles can be accumulated into layers perpendicular to the propagation direction of the wave and the strength of the layering can be triggered by the speed of the wave. In particular, this effect occurs for nonsinusoidal, "ramplike" external potential with sharp edges, while it does not occur for a sinusoidal one.

The second goal of this paper is to calculate the resistance of sheared colloidal layers. A microscopic understanding of shear flow near interfaces is still in its infancy. While kinetic theories have had some success in gases (see Ref. [21] for a review), it is more difficult to construct a theory for a sheared

dense liquid on the molecular scale [22,23]. Even the question regarding the choice of the hydrodynamic boundary conditions that are appropriate on a molecular scale is still intensely debated [24–30]. In this paper, we investigate the colloidal counterpart of this problem. The difference in our case is the Brownian motion of the particles in the quiescent solvent, which is different from ordinary Newtonian dynamics performed by molecules. We show that dynamical density functional theory provides a "microscopic" approach to shear resistance. In particular, we consider two parallel repulsive walls with a periodic topographical substructure, which are moving relative to each other. One stays quiescent with the solvent that contains the colloidal particles, whereas the other is pulled with a constant speed v through the suspension. The relative friction induced by the sheared colloidal particles is calculated using dynamical density functional theory (DDFT) and compared to Brownian dynamics computer simulation. We find good agreement, demonstrating that dynamical density functional theory provides a molecular platform for a theory of shear resistance. We also predict a nonmonotonic dependence of the shear resistance for confined suspensions as a function of the speed of the second wall.

The paper is organized as follows: in Sec. II, we briefly define the dynamical density functional approach. Details of the computer simulation procedure are summarized in Sec. III. Results for a traveling wave external potential are presented in Sec. IV. Sheared colloids between topographical structured walls are considered in Sec. V. Finally, we conclude in Sec. VI.

II. DYNAMICAL DENSITY FUNCTIONAL THEORY

We consider an assembly of N Brownian particles, such as colloids in a microscopic solvent, whose coordinates are $\{\mathbf{r}_1,\mathbf{r}_2,\ldots,\mathbf{r}_N\}$ and which interact via an arbitrary pair potential $V(r)$. They are kept at finite temperature T and possess a mean number density ρ. In addition, the colloids are under the influence of a time-dependent external potential $V_{\text{ext}}(\mathbf{r},t)$. DDFT does not incorporate hydrodynamic interactions. Therefore, we handle them in our studies in the following way. A major effect of hydrodynamic interactions can be simply encaptured by a rescaling of the drag coefficient into an effective one; this was demonstrated by Medina-Noyola [34]. Using this scaling, hydrodynamic interactions can be taken into consideration in our treatment and will therefore just renormalize the time scale. More sophisticated analysis shows that corrections due to hydrodynamic interactions are of the order of $\frac{3}{2}C^2\phi^{1/3}$, where $C=\bar{r}\phi^{1/3}/a$, $\bar{r}$ is the mean interparticle spacing, a is the physical core size, $\sigma/2$ is the interaction radius, and $\phi=(4\pi/3)\rho a^3$ is the volume fraction [31–33]. In our studies we have typically $\bar{r}\approx\sigma$ and $\rho=1/\sigma^3$. Insertion yields a corrections of the order of $6(\sigma/2a)^2\phi=2\pi a/\sigma$. Therefore, our treatment applies to particles with small physical core size a but large interaction radius $\sigma/2$. There are several examples for such particles—e.g., stiff polyelectrolyte stars, tetrapods, star-polymers, and dendrimers—which fulfill these conditions. The particles' equations of motion read as

$$\frac{\mathrm{d}\mathbf{r}_i(t)}{\mathrm{d}t}=-\Gamma\nabla_{\mathbf{r}_i}\left(\sum_{j\neq i}V(|\mathbf{r}_i-\mathbf{r}_j|)+V_{\text{ext}}(\mathbf{r}_i,t)\right)+\mathbf{w}_i(t), \quad (1)$$

where Γ is a mobility coefficient and $\mathbf{w}_i(t)=(w_i^x,w_i^y,w_i^z)$ is a stochastic Gaussian noise term representing the random collisions with the solvent molecules and having the properties

$$\langle\mathbf{w}_i(t)\rangle=0,\quad \langle w_i^\alpha(t)w_i^\beta(t')\rangle=2D\delta_{\alpha\beta}\delta(t-t'). \quad (2)$$

In Eq. (2) above $\langle\cdots\rangle$ denotes the average over the Gaussian noise distribution, $\alpha,\beta=x,y,z$ are the Cartesian components, and D is the diffusion coefficient for which the Einstein relation gives $\Gamma/D=(k_BT)^{-1}\equiv\beta$, where k_BT is the thermal energy. Moreover, for hard spheres of radius a in a fluid of viscosity η, the Stokes relation $\Gamma=1/6\pi\eta a$ holds. Applying the rules of the Itô stochastic calculus, Marini Bettolo Marconi and Tarazona [10] transformed the above equation into

$$\Gamma^{-1}\frac{\partial\rho(\mathbf{r},t)}{\partial t}=\nabla_{\mathbf{r}}\cdot\left(\beta^{-1}\nabla_{\mathbf{r}}\rho(\mathbf{r},t)+\rho(\mathbf{r},t)\nabla_{\mathbf{r}}V_{\text{ext}}(\mathbf{r},t)+\int\mathrm{d}\mathbf{r}'\langle\hat{\rho}(\mathbf{r},t)\hat{\rho}(\mathbf{r}',t)\rangle\nabla_{\mathbf{r}}V(|\mathbf{r}-\mathbf{r}'|)\right). \quad (3)$$

Here, $\hat{\rho}(\mathbf{r},t)=\Sigma_i\delta(\mathbf{r}_i(t)-\mathbf{r})$ is the usual one-particle density operator and $\rho(\mathbf{r},t)=\langle\hat{\rho}(\mathbf{r},t)\rangle$ is its noise average. Equation (3) is exact, but it is not a closed relation, because in order to obtain $\rho(\mathbf{r},t)$ one needs the equal-time two-particle correlation $\rho^{(2)}(\mathbf{r},\mathbf{r}',t)\equiv\langle\hat{\rho}(\mathbf{r},t)\hat{\rho}(\mathbf{r}',t)\rangle$. Marini Bettolo Marconi and Tarazona [10] suggested the following physical assumption to obtain a closure that opens a connection to the density functional formalism: as the system follows its relaxation dynamics, the instantaneous two-particle correlations are approximated by those of a system in thermodynamic equilibrium with a *static* one-particle density $\rho(\mathbf{r})$ that is the same as the instantaneous, noise-averaged one-particle density $\rho(\mathbf{r},t)$. Then Eq. (3) can be cast into a form involving exclusively the equilibrium density free energy functional $F[\rho]$ as

$$\Gamma^{-1}\frac{\partial\rho(\mathbf{r},t)}{\partial t}=\nabla\cdot\left[\rho(\mathbf{r},t)\nabla\frac{\delta F[\rho(\mathbf{r},t)]}{\delta\rho(\mathbf{r},t)}\right]. \quad (4)$$

This is the central equation of DDFT. In Eq. (4), the free energy functional is given by [8]

$$F[\rho]=\beta^{-1}\int\mathrm{d}\mathbf{r}\rho(\mathbf{r})\{\ln[\Lambda^3\rho(\mathbf{r})]-1\}+\int\mathrm{d}\mathbf{r}\rho(\mathbf{r})V_{\text{ext}}(\mathbf{r},t)+F_{\text{ex}}[\rho], \quad (5)$$

where Λ is the (irrelevant) de Broglie thermal wavelength and $F_{\text{ex}}[\rho]$ is the excess free energy functional. Equation (4) has the form of a continuity equation with the current

$$\mathbf{j}(\mathbf{r},t)\equiv-\Gamma\rho(\mathbf{r},t)\nabla\left.\frac{\delta F[\rho(\mathbf{r},t)]}{\delta\rho(\mathbf{r},t)}\right|_{\rho(\mathbf{r},t)}=-\Gamma\rho(\mathbf{r},t)\nabla\mu(\mathbf{r},t), \quad (6)$$

where $\mu(\mathbf{r},t)$ is a "nonequilibrium local chemical potential" that reduces to the equilibrium value in the absence of time-dependent external potentials as Archer and Evans have shown [35]. They proposed an alternative (and more general)

derivation, which is based on the Smoluchowski equation. Thereby they have shown that the result (6) is also valid in the presence of many-body potentials.

In this work, we assume an ultrasoft Gaussian pair potential between the interacting particles:

$$V(|\mathbf{r}-\mathbf{r}'|) = \epsilon \exp[-(|\mathbf{r}-\mathbf{r}'|/\sigma)^2]. \tag{7}$$

The Gaussian pair potential has been shown to be a realistic description for solutions of polymer coils [36], low-arm star polymers [37], dendrimers [19], and weakly charged polyelectrolyte chains [38]. It is also realized for hairy micelles in a good solvent and for colloids stabilized by long grafted polymer chains. For the sake of convenience, we set $\epsilon = k_B T$, providing the energy unit of the system, whereas σ, which corresponds to the gyration radius in a polymer realization of the Gaussian potential, will be the unit of length henceforth. Accordingly, the natural time scale of the problem, providing the unit of time in this work is the Brownian time scale $\tau_B = \sigma^2/(\epsilon\Gamma)$.

For Gaussian particles, the *mean-field* or *random-phase approximation* (RPA) functional $F_{ex}[\rho]$ has been shown to be very accurate for static properties [16–18,39–43]. It is indeed an excellent approximation for both the bulk and interfacial structure of Gaussian systems, whose validity increases as the concentration of the system becomes higher. This has been adequately and repeatedly demonstrated in the literature (see again [16,39,40]). It reads as

$$F_{ex}[\rho] = \frac{1}{2}\int\int d\mathbf{r}d\mathbf{r}' V(|\mathbf{r}-\mathbf{r}'|)\rho(\mathbf{r})\rho(\mathbf{r}'). \tag{8}$$

Inserting Eq. (8) into Eq. (4) yields

$$\Gamma^{-1}\frac{\partial\rho(\mathbf{r},t)}{\partial t} = \beta^{-1}\nabla_{\mathbf{r}}^2\rho(\mathbf{r},t) + \nabla_{\mathbf{r}}\rho(\mathbf{r},t)\cdot\int d\mathbf{r}'\nabla_{\mathbf{r}}V(|\mathbf{r} - \mathbf{r}'|)\rho(\mathbf{r}',t) + \rho(\mathbf{r},t)\int d\mathbf{r}'\nabla_{\mathbf{r}}^2 V(|\mathbf{r}-\mathbf{r}'|)\rho(\mathbf{r}',t) + \nabla_{\mathbf{r}}\rho(\mathbf{r},t)\cdot\nabla_{\mathbf{r}}V_{ext}(\mathbf{r},t) + \rho(\mathbf{r},t)\nabla_{\mathbf{r}}^2 V_{ext}(\mathbf{r},t). \tag{9}$$

Given an initial density field $\rho(\mathbf{r},t=0)$ and a prescribed external potential $V_{ext}(\mathbf{r},t)$, Eq. (9) can be solved numerically to obtain $\rho(\mathbf{r},t)$.

Two situations are considered subsequently both of which are characterized by different time-dependent external potentials. (i) First, a traveling wave corresponds to a potential that only depends on one coordinate in the form

$$V_{ext}(\mathbf{r},t) = \Phi\left(\frac{2\pi}{\lambda}(z-vt)\right), \tag{10}$$

where the wave envelope function $\Phi(\phi)$ is 2π periodic in its argument ϕ and λ is the wavelength. For simplicity, we only consider cases where $\lambda=\sigma$. Furthermore, v is the velocity of the traveling wave. An additional parameter to be specified is the conserved averaged number density ρ_0. In all of our studies, we choose $\rho_0\sigma^3=1$. In this case of densities close to overlap, the RPA functional is justified [16,17].

The second case (ii) consists of two parallel repulsive walls with a periodic topographical substructure which are moving relatively to each other inducing a shearing in the suspension. The external in this case reads as

$$V_{ext}(\mathbf{r},t) = \Phi_w(x, 2\pi y/\lambda) + \Phi_w(L-x, 2\pi(y-vt)/\lambda), \tag{11}$$

where the static single wall potential $\Phi_w(x,\phi)$ is 2π periodic in its argument ϕ. Here, x is the coordinate perpendicular to the walls, L is the wall distance, y is the coordinate directed along the periodic wall structure of wavelength λ, and v is the speed of the second wall. A sketch of the second setup is presented in Fig. 4, below. In this case, the conserved total number density which is defined as the averaged number of particle in the total volume is again chosen to be $\rho_0\sigma^3=1$.

III. NUMERICAL DETAILS

A. Brownian dynamics computer simulation

Brownian dynamics (BD) simulations of Eq. (1) are straightforward to carry out. For case (i) we use a cubic box with periodic boundary conditions in all three directions. The length of the simulation box is a multiple of the wavelength. In case (ii) the system is periodically repeated in the two lateral directions only. The number of Brownian particles in the box is around $N_B=1000$, so that the simulations are free from finite-size effects. The Langevin equations of motion including the external field are numerically solved using a finite time step $\Delta t=0.002\tau_B$ in all simulations, together with the technique of Ermak [44,45]. In order to obtain the time-dependent density $\rho(\mathbf{r},t)$ we perform a large number N_{run} of independent runs with different initial configurations, typically $N_{run}=5000$, sampled from a situation with a static external potential. We checked that after a sufficiently long time of roughly $t=5\tau_B$, the system runs into the same steady state for all initial configurations chosen.

B. Forward-time centered space algorithm

The partial differential equation of time evolution (9) is solved numerically employing the forward-time centered space (FTSC) algorithm [46]. This method employs a finite-difference approximation to solve the initial-value problem and requires appropriate boundary conditions. In the first setup, the traveling wave, we use periodic boundary conditions since the applied potential is itself periodic. In the second setup, the sheared walls, we use periodic boundary conditions in the direction in which the wall is moving and set the density to zero outside the walls. Thus, we do not impose any artificial boundary effects. Since the applied difference scheme is only accurate to the first order in Δt, we use a small time step $\Delta t=10^{-6}\tau_B$ when solving Eq. (9) to achieve sufficient accuracy.

IV. TRAVELING WAVE POTENTIAL

We now present the results obtained for the steady state in the case of the traveling wave potential. The particles are pulled in one direction across the system, as in Refs. [47,48], where hydrodynamic interactions are ignored as well. The

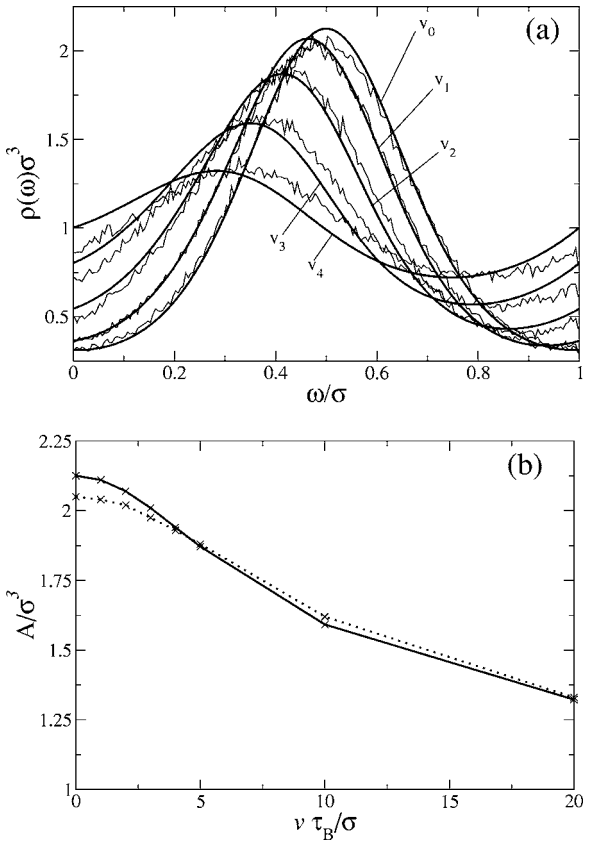

FIG. 1. (a) DDFT (solid, thick curves) and BD (noisy curves) results for the steady-state density profiles $\rho(\omega)$, $\omega=z-vt$ (formally at $t=0$), under the influence of the external potential of Eq. (12) for the following velocities: $v_0=0$, $v_1=2.0\sigma/\tau_B$, $v_2=5\sigma/\tau_B$, $v_3=10\sigma/\tau_B$, and $v_4=20\sigma/\tau_B$. (b) Amplitude A of the density profile from theory (solid line) and simulation (dotted line).

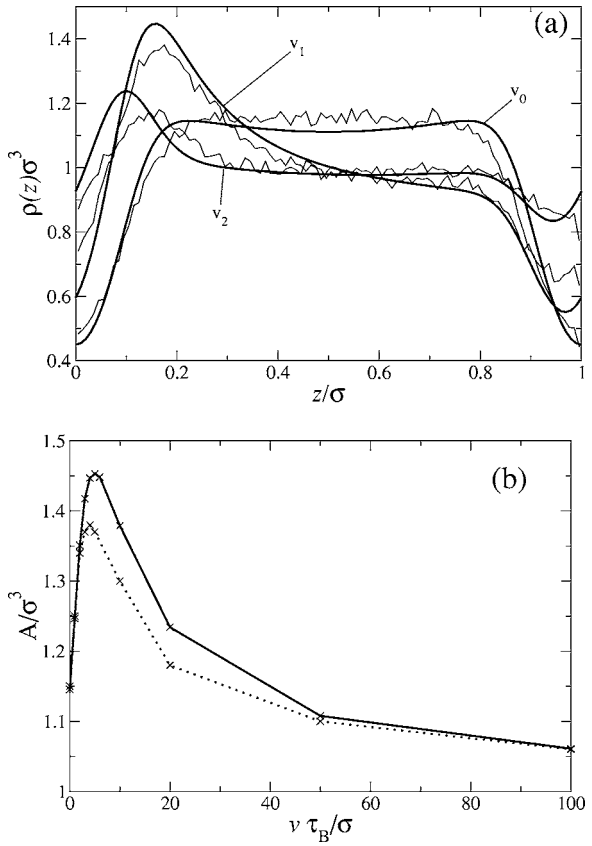

FIG. 2. Same as Fig. 1 but now for the traveling wave potential of Eq. (14). (a) DDFT (solid, thick curves) and BD (noisy curves) results for the steady-state density profiles for $v_0=0$, $v_1=5\sigma/\tau_B$, and $v_2=20\sigma/\tau_B$. (b) Amplitude A of the density profile from theory (straight line) and simulation (dotted line).

first envelope function that we consider is a pure sinusoidal one—i.e.,

$$V_{\text{ext}}(\mathbf{r},t)=\phi_0\sin\left[\frac{2\pi}{\lambda}(z-vt)\right], \tag{12}$$

where ϕ_0 sets the amplitude of the traveling wave. In what follows we also define the variable

$$\omega=z-vt. \tag{13}$$

We choose $\phi_0=k_BT$. In the fluid state, the steady state possesses a dynamical one-particle density field that depends only on the variable ω. In Fig. 1(a) the steady-state density profiles of the Brownian particles in a quiescent solvent are shown for different velocities v of the traveling wave, Eq. (12). For zero velocity, this profile is a true equilibrium density profile in a periodic external potential which was studied earlier in the context of laser-induced freezing [5]. A finite traveling speed of the wave reduces the amplitude of the steady-state density profile until a homogeneous distribution is achieved in the limit $v\to\infty$. In fact, for very high velocities the Brownian particles do not respond to the external potential because the changes in the potential are too fast for them to follow; hence, they do not experience any force on average. The amplitude A of the steady-state density profiles as defined by its maximum as a function of z is shown in Fig. 1(b) as a function of the velocity v. As can be seen, it decays monotonically in v. Finally, for all speeds considered here, we find very good agreement between theory and simulation, proving that the DDFT is an accurate theory.

Next we consider a wave with a *ramplike* envelope, as modeled by the following external potential:

$$V_{\text{ext}}(z-vt)=\phi_0\sin^{20}\left[\frac{\pi}{\lambda}(z-vt)\right]. \tag{14}$$

The corresponding steady-state density profiles with its amplitudes are presented in Fig. 2(a). In this case, we observe a qualitative difference of the amplitude A as a function of the velocity v to the sinusoidal case. At the moving ramp, particles pile up. This effect is destroyed, however, for very large velocities. Consequently, there is a *nonmonotonicity* in the density amplitude as a function of the speed as shown in Fig. 2(b). This may be exploited to produced a tailored layering of particles by a suitably moving traveling wave. Again, we find good agreement between theory and simulation.

Let us now describe a simple "minimal" theory in order to understand the nonmonotonic variation of the amplitude with

the velocity v. First, we neglect the interparticle interactions completely. This approximation is valid, of course, only for small densities. For ultrasoft interactions, it works also for very high densities [16–18,39–42]; hence, it is expected to work at least qualitatively for the case at hand. The equation of motion (1) for a single colloidal particle i then simplifies to

$$\frac{\mathrm{d}\mathbf{r}_i(t)}{\mathrm{d}t} = -\Gamma\nabla_{\mathbf{r}_i} V_{\mathrm{ext}}(z_i - vt) + w_i(t). \tag{15}$$

Transforming into new coordinates $\tilde{\mathbf{r}}_i = \mathbf{r}_i - vt\hat{\mathbf{e}}_z$ the new equations read

$$\frac{\mathrm{d}\tilde{\mathbf{r}}_i(t)}{\mathrm{d}t} = -\Gamma\nabla_{\tilde{\mathbf{r}}_i} \tilde{V}_{\mathrm{ext}}(\tilde{z}_i) + w_i(t), \tag{16}$$

with a new unbounded static potential $\tilde{V}_{\mathrm{ext}}(z) = V_{\mathrm{ext}}(z) - vz/\Gamma$, which is a consequence of the nonequilibrium situation. If we just ignore this and study a static situation over one periodicity length of $V_{\mathrm{ext}}(z)$, the density profile of an ideal gas is $1/\mathcal{N}\exp[-\beta\tilde{V}_{\mathrm{ext}}(\tilde{z}_i)]$, where the prefactor $\mathcal{N} = \int_0^\lambda \mathrm{d}z \exp[-\beta\tilde{V}_{\mathrm{ext}}(\tilde{z})]/\rho_0$ guarantees correct normalization. While this is a reasonable description close to the ramp, the periodicity condition $\rho(z=0) = \rho(z=\lambda)$ is violated. We impose this condition by subtracting the offset as follows:

$$\rho(z) = \frac{1}{\lambda}(c_0 - c_\lambda)\left(z - \frac{\lambda}{2}\right) + \frac{1}{\mathcal{N}}\exp[-\beta\tilde{V}_{\mathrm{ext}}(z)], \tag{17}$$

with $c_0 = 1/\mathcal{N}\exp[-\beta\tilde{V}_{\mathrm{ext}}(0)]$ and $c_0 = 1/\mathcal{N}\exp[-\beta\tilde{V}_{\mathrm{ext}}(\lambda)]$. Expression (17) ensures correct normalization and periodicity of the steady-state density profile: $\rho(0) = \rho(\lambda) = (c_0 + c_\lambda)/2$. A comparison of the full DDFT results is shown in Fig. 3(a). It becomes evident from Fig. 3(b) that the simple expression (17) is capable of predicting the nonmonotony of the density amplitude as a function of speed v in a qualitative but not in a quantitative way. It is only for small velocities v that the full density profiles are in quantitative agreement with the simulation or DDFT data.

V. COLLOIDS SHEARED BETWEEN TWO TOPOGRAPHICALLY STRUCTURED WALLS CREATED BY LASER-OPTICAL FIELDS

In this section we consider a setup that consists of two parallel repulsive walls, each decorated with a periodic topographical substructure (see Fig. 4). One of the walls is moving relatively to the other, inducing a shearing in the suspension, whereas the other one stays quiescent with the solvent. Here, the solvent is at rest; the moving wall only interacts with the Gaussian particles, as realized for moving laser-optical fields. Therefore, the walls are completely penetrable for the solvent. The external potential is of the form (11) with the single static wall potential given by

$$\Phi_{\mathrm{w}}(x,\phi) = \Phi_0 \exp\left(-\frac{x}{X_0 + a\sin\phi}\right). \tag{18}$$

Here Φ_0 sets the interaction strength, X_0 is a length scale, and a is the amplitude of the topographical wall structure.

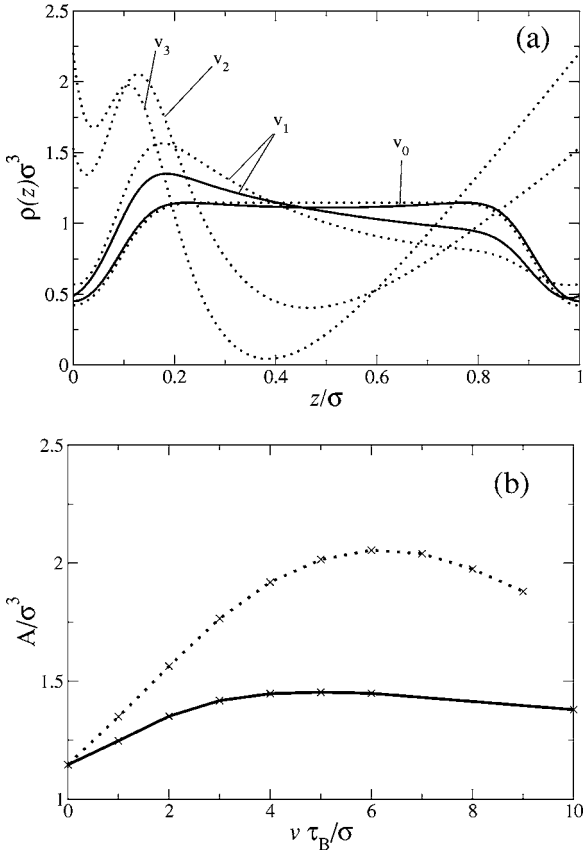

FIG. 3. (a) DDFT results (solid curves) and results from the ideal gas theory (dashed curves) for the steady-state density profiles of a system under the influence of the traveling wave potential of Eq. (14). The velocities of the external potential $v_0 = 0\sigma/\tau_{\mathrm{B}}$, $v_1 = 2\sigma/\tau_{\mathrm{B}}$, $v_2 = 6\sigma/\tau_{\mathrm{B}}$, and $v_3 = 8\sigma/\tau_{\mathrm{B}}$. (b) Amplitude A of the density profile from DDFT (solid curve) and from the ideal gas theory (dashed curve). We find a nonmonotonic behavior in both cases

The walls are moving relatively to the one another, and the system evolves in time. However, due to the periodic topography, the system repeats itself after the time period $T = \lambda/v$. Thus we define a steady-state situation when the following equality is fulfilled: $\rho(x,y,t) = \rho(x,y,t+T)$. Since the density

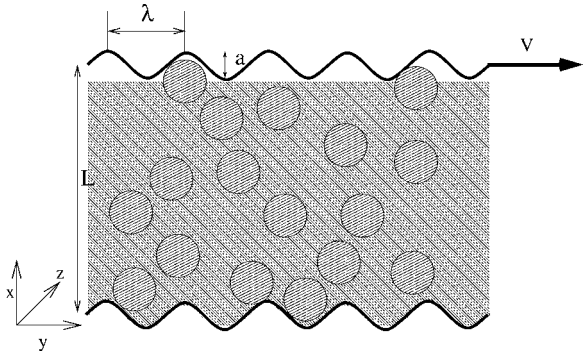

FIG. 4. Schematic top view of the system with two walls moving relatively to each other modeled via the potential (11). If the upper wall is moving sufficiently fast, the particles cannot penetrate into the unhatched area. The system is infinitely extended in both the y and z directions.

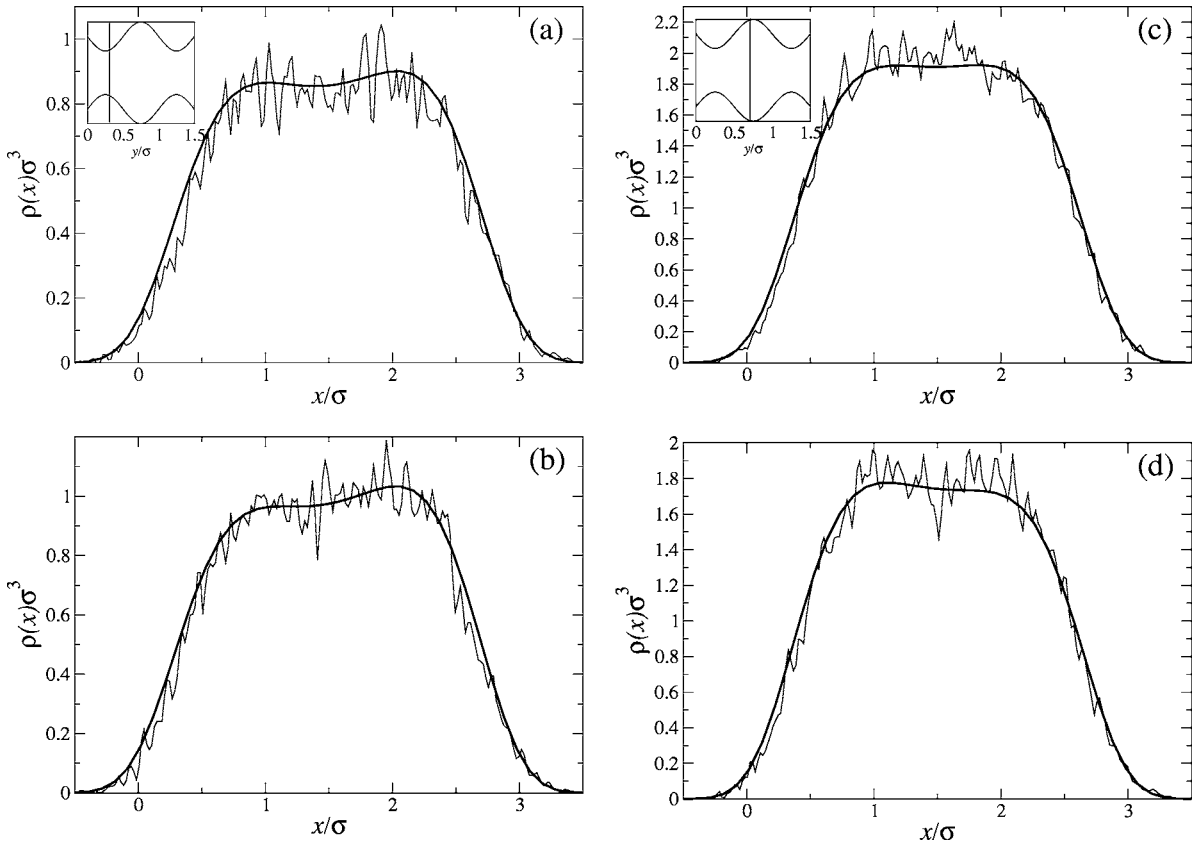

FIG. 5. Cuts through the DDFT (solid curves) and BD (noisy curves) results for the steady-state density profiles of a Brownian fluid sheared via Eq. (11) for $L=3\sigma$, $y=0.3\sigma$, and (a) $v=5.0\sigma/\tau_B$ and (b) $v=15.0\sigma/\tau_B$ and, for $y=0.7\sigma$, (c) $v=5.0\sigma/\tau_B$ and (d) $v=15.0\sigma/\tau_B$. The inset shows the instantaneous position of the wall (wavy lines) and the position of which a cut is taken (straight line).

profiles depend on coordinates x and y, the BD results can be averaged only over the z direction. Thus they are noisier than those in the previous section, where a second direction can be used to average. For this reason, we do not present the whole three-dimensional BD steady-state density profiles. Instead we show several cuts through the densities along the x coordinate. To improve the statistics of the BD density profiles for the above-mentioned reason and thus to reduce the noise, we average the DDFT and BD steady-state density profiles over a slice of width $\Delta y=0.3\lambda$ in the y direction. The cuts are shown in Figs. 5 and 6. All presented plots are for the case that the topographical substructures of the two walls are phase shifted by π. The velocities are chosen as $v=5\sigma/\tau_B$ and $v=15\sigma/\tau_B$, the positions of the cuts are $y_1=0.3\lambda$ and $y_2=0.7\lambda$ in the frame of rest of the quiescent wall, and the distances between the walls are $L=3\sigma$ (Fig. 5) and $L=10\sigma$ (Fig. 6). The other parameters are chosen as follows: $\Phi_0=10k_BT$, $\lambda=X_0=\sigma$, and $a=X_0/10=0.1\sigma$. The conserved total number density is again chosen to be $\rho_0\sigma^3=1$.

As revealed by Figs. 5 and 6 we find very good agreement between theory and simulation and demonstrate thereby that the DDFT is an adequate molecular theory to describe the shearing of a Brownian fluid. The density profiles in Figs. 5 and 6 are not symmetric; this effect is due to the motion of the wall. For higher velocities v of the wall, this asymmetry is more distinctive—e.g., Figs. 5(b) and 5(d). This can be explained by the fact that for higher velocities the particles are accumulated on the increasing side of the wall and depleted in the valleys of the external potential, whereas in the quiescent case the density profile is symmetric. The same effect can be seen in the previous section in Fig. 1, where position of the maxima of the density profile with respect to the wave field is moving in the opposite direction of the velocity for increasing velocities. The large difference in the maximal values of the density in Fig. 5 is due to fact that the walls are repulsive. In the case of Figs. 5(a) and 5(b) the particles are squeezed into the region, where the cuts in Figs. 5(c) and 5(d) are taken. In the case $L=10\sigma$ this effect is less distinctive.

To calculate a shear resistance originating from the Brownian fluid we average the force $\mathbf{F}_D$ per area exerted by the particle on the walls in the steady state. A suitable time average for this force is

$$\mathbf{F}_D = -\lim_{\tau\to\infty}\frac{1}{\tau}\int_0^\tau \int_{-\infty}^{+\infty}\int_0^\lambda dt dx dy \rho(x,y,t)\,\nabla V_{ext}(x,y,t). \tag{19}$$

This formula can directly be can evaluated both in the numerical implementation of the DDFT and in the BD simulations. By symmetry, $\mathbf{F}_D$ vanishes in the z direction, perpendicular to the velocity. Its component perpendicular to the wall gives insight into the wall pressure. Here, we are interested in the component $F_D^{(y)}$ along the shearing direction, par-

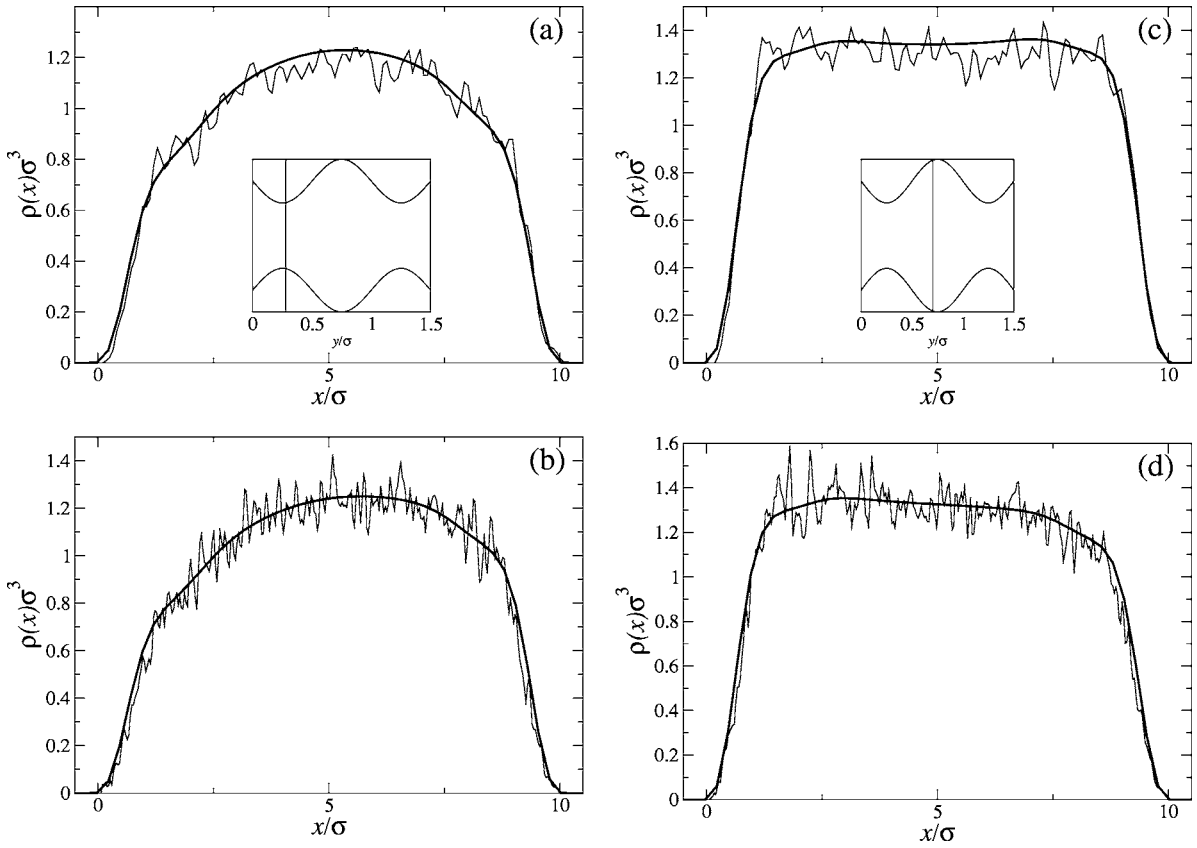

FIG. 6. Same as Fig. 5 but now for $L=10\sigma$, $y=0.3\sigma$, and (a) $v=5.0\sigma/\tau_B$ and (b) $v=15.0\sigma/\tau_B$ and, for $y=0.7\sigma$, (c) $v=5.0\sigma/\tau_B$ and (d) $v=15.0\sigma/\tau_B$.

allel to the velocity. We have studied how the resistance force $F_D^{(y)}$ behaves as a function of the velocity v. The BD simulation and DDFT results are depicted in Fig. 7. A sublinear behavior is revealed for increasing velocities v. There is a nonmonotonic behavior for increasing v. This can be understood qualitatively by the fact that for large velocities the particles will be squeezed into the regions where they are not hindered at all by the moving plate (see the hatched area in Fig. 4). The maximum is reached for similar velocities, regardless of whether the system is strongly confined or not,

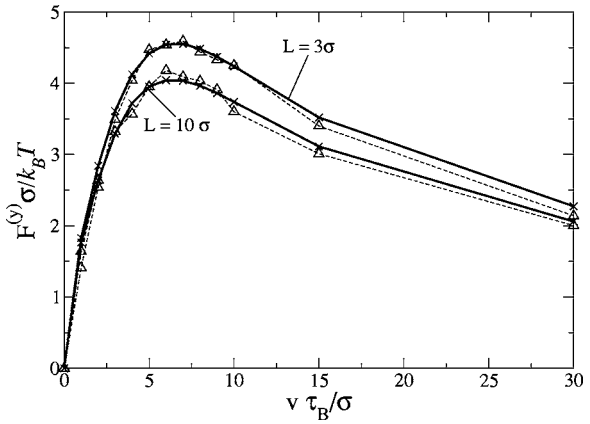

FIG. 7. DDFT results (solid curves) and BD results (dashed curves) of the y component of the resistance force, Eq. (19), as a function of v for $L=3\sigma$ and $L=10\sigma$.

as can be deduced from a comparison between the $L=3\sigma$ and $L=10\sigma$ cases. This friction is qualitatively different from turbulent aerodynamics and hydrodynamics where one typically gets a crossover from a friction linear in v to a superlinear quadratic law $\propto v^2$. Furthermore, the friction increases for strong confinement; the difference is entirely caused by the relative shearing. This clearly points to a significant viscosity increase of confined liquids under shear. As stated earlier, we have assumed a small physical core size a of the particles with respect to the interaction radius $\sigma/2$. Therefore, there is no considerable shear flow induced on the solvent by the motion of the Gaussian particles. As long as $a \ll \sigma$, as is the case here, hydrodynamic interactions can be ignored, implying that there is no considerable solvent backflow in the system. For completeness, however, we briefly discuss the case $a \approx \sigma$. Under such a condition, in the steady state, the colloids will generate a linear shear flow in the solvent through their collisions with the solvent particles. In this case, the solvent particles will assume a linear velocity profile associated with a corresponding stress in the fluid, $\eta v/L$, that exerts an additional force on the Gaussian particles. The stress-induced force per particle then reads $F_s(v)=\eta\sigma^2 v/L$. But even in this case, the force originating from the shear flow in the solvent is small compared to the force reported in Fig. 7. In order to quantify this, we consider the ratio of the two forces at a velocity $v=6\sigma/\tau_B$, which corresponds to the maximum of F_D^y. From Fig. 7 we read off F_D^y and the ratio reads

$$\frac{F_D^{(y)}}{F_s} = \frac{4k_BT/\sigma}{\eta\sigma^2 6\sigma/(\tau_B L)} = \frac{4\pi La}{\sigma^2} \approx \frac{4\pi L}{\sigma}. \quad (20)$$

From Eq. (20) above, it becomes evident that even if a is comparable to σ the force reported in Fig. 7 is at least one order of magnitude larger than the force that will arise from a flow in the solvent for the distances L of the walls regarded.

VI. CONCLUSIONS

Soft colloidal particles exposed to external time-dependent fields exhibit a variety of new effects which are not known from equilibrium properties. Among those we described a nonlinear variation of the steady-state density amplitude as a function of the velocity of the traveling wave field for a ramplike envelope function of the wave. Furthermore, we obtained a sublinear behavior of the friction exerted by the colloidal particles on a moving structured wall. All these effects can in principle be observed in real-space experiments of colloidal suspensions in laser-optical fields. We think that the effects are general and are not due to the specific form used for the interactions and the special combinations of parameters investigated in this paper.

As mentioned in Sec. II, our approach neglects hydrodynamic interactions, an approximation that is well justified for systems bearing the physical characteristics put forward there. Yet for general colloidal suspensions, hydrodynamic interactions are relevant. An alternative method that has been recently expanded in order to include hydrodynamic effects is that of phase field models [49]. In particular, Anderson *et al.* [50,51] as well as Tönhardt and Amberg [52] have coupled phase-field equations with the Navier-Stokes equation of hydrodynamics, in an attempt to take proper account of the convection present in the fluid phase during the process of growth of a solid interface. This problem is clearly distinct from the situation of shearing which is the subject of this work. Moreover, whereas in our work the contact with the microscopic interactions between the constituent particles remains intact, in phase-field models the spatiotemporal evolution of the coarse-grained density is described on the basis of phenomenological free energy models.

Our results also indicate that the dynamical density functional theory is capable of describing the steady state even in situations of large speeds. It would be interesting to apply this theory to more complicated dynamical situations such as transport phenomena and full time-dependent processes such as transport of particles through porous media and nanochannels.

ACKNOWLEDGMENTS

Discussions with J. L. Barrat, S. U. Egelhaaf, and H. Tanaka are gratefully acknowledged. This work is supported by the Deutsche Forschungsgemeinschaft within SFB TR6 (project section C3).

[1] M. Sullivan, K. Zhao, C. Harrison, R. H. Austin, M. Megens, A. Hollingsworth, W. B. Russel, Z. Cheng, T. Mason, and P. M. Chaikin, J. Phys.: Condens. Matter **15**, S11 (2003).
[2] H. Löwen, J. Phys.: Condens. Matter **13**, R415 (2001).
[3] J. Dzubiella, G. P. Hoffmann, and H. Löwen, Phys. Rev. E **65**, 021402 (2002).
[4] C. Bechinger, J. Phys.: Condens. Matter **13**, R321 (2001).
[5] C. Bechinger, Curr. Opin. Colloid Interface Sci. **7**, 204 (2002).
[6] C. Bechinger, M. Brunner, and P. Leiderer, Phys. Rev. Lett. **86**, 930 (2001).
[7] C. Bechinger, Q. H. Wei, and P. Leiderer, J. Phys.: Condens. Matter **12**, A425 (2000).
[8] H. Löwen, Phys. Rep. **237**, 249 (1994).
[9] Y. Rosenfeld, M. Schmidt, H. Löwen, and P. Tarazona, Phys. Rev. E **55**, 4245 (1997).
[10] U. Marini Bettolo Marconi and P. Tarazona, J. Chem. Phys. **110**, 8032 (1999); J. Phys.: Condens. Matter **12**, A413 (2000).
[11] J. Dzubiella and C. N. Likos, J. Phys.: Condens. Matter **15**, L147 (2003).
[12] M. Rex, C. N. Likos, and H. Löwen (unpublished).
[13] A. J. Archer, J. Phys.: Condens. Matter **17**, 1405 (2005).
[14] K. Fuchizaki and K. Kawasaki, J. Phys.: Condens. Matter **14**, 12203 (2002).
[15] G. K.-L. Chan and R. Finken, Phys. Rev. Lett. **94**, 183001 (2005).
[16] C. N. Likos, A. Lang, M. Watzlawek, and H. Löwen, Phys. Rev. E **63**, 031206 (2001).
[17] A. Lang, C. N. Likos, M. Watzlawek, and H. Löwen, J. Phys.: Condens. Matter **12**, 5087 (2000).
[18] A. A. Louis, P. G. Bolhuis, and J-P. Hansen, Phys. Rev. E **62**, 7961 (2000).
[19] C. N. Likos, M. Schmidt, H. Löwen, M. Ballauff, D. Pötschke, and P. Lindner, Macromolecules **34**, 2914 (2001); C. N. Likos, S. Rosenfeld, N. Dingenouts, M. Ballauff, N. Werner, and F. Vögte, J. Chem. Phys. **117**, 1869 (2002).
[20] H. Tanaka *et al.*, (private communication).
[21] V. Garzo and A. Santos, *Kinetic Theory of Gases in Shear Flow, Fundamental Theories of Physics*, Vol. 131 (Kluwer, Dordrecht, 2003).
[22] J. F. Lutsko, Phys. Rev. E **66**, 051109 (2002).
[23] J. F. Lutsko and J. W. Dufty, Phys. Rev. E **66**, 041206 (2002).
[24] M. O. Robbins and M. H. Müser, in *Handbook of Modern Tribology*, edited by Bharat Bhushan (CRC Press, Boca Raton, 2001).
[25] L. Bocquet and J. L. Barrat, Phys. Rev. Lett. **70**, 2726 (1993).
[26] J. L. Barrat and L. Bocquet, Phys. Rev. Lett. **82**, 4671 (1999).
[27] P. A. Thompson and S. M. Troian, Nature (London) **389**, 360 (1997).
[28] M. J. Stevens, M. Mondello, G. S. Grest, S. T. Chui, H. D. Cochran, and P. T. Cummings, J. Chem. Phys. **106**, 7303 (1997).
[29] M. Cieplak, J. Koplik, and J. R. Banavar, Phys. Rev. Lett. **86**, 803 (2000).
[30] M. Cieplak, J. Koplik, and J. R. Banavar, Physica A **274**, 8281

(1999).
[31] G. Nägele, B. Steininger, U. Genz, and R. Klein, Phys. Scr. **55**, 119 (1994).
[32] J. K. G. Dhont, *An Introduction to Dynamics of Colloids* Amsterdam, (Elsevier, 1996).
[33] W. B. Russel, D. A. Saville, and W. R. Schowalter, *Colloidal Dispersions* (Cambridge University Press, Cambridge, England, 1989).
[34] M. Medina-Noyola, Phys. Rev. Lett. **60**, 2705 (1988).
[35] A. J. Archer and R. Evans, J. Chem. Phys. **121**, 4246 (2004).
[36] A. A. Louis, P. G. Bolhuis, J. P. Hansen, and E. J. Meijer, Phys. Rev. Lett. **85**, 2522 (2000).
[37] A. Jusufi, J. Dzubiella, C. N. Likos, C. von Ferber, and H. Löwen, J. Phys.: Condens. Matter **13**, 6177 (2001).
[38] M. Konieczny, C. N. Likos, and H. Löwen, J. Chem. Phys. **121**, 4913 (2004).
[39] A. J. Archer and R. Evans, Phys. Rev. E **64**, 041501 (2001).
[40] A. J. Archer and R. Evans, J. Phys.: Condens. Matter **14**, 1131 (2002).
[41] A. J. Archer, C. N. Likos, and R. Evans, J. Phys.: Condens. Matter **14**, 12031 (2002).
[42] A. J. Archer, R. Evans, and R. Roth, Europhys. Lett. **59**, 526 (2002).
[43] A. J. Archer, C. N. Likos, and R. Evans, J. Phys.: Condens. Matter **16**, L297 (2004).
[44] D. L. Ermak, J. Chem. Phys. **62**, 4189 (1975).
[45] M. P. Allen and T. J. Tildesley, *Computer Simulation of Liquids* (Clarendon, Oxford, 1989).
[46] W. H. Press, S. A. Teukolosky, W. T. Vetterling, and B. P. Flannery, *Numerical Recipes in C* (Cambridge University Press, Cambridge, England, 1995).
[47] C. Reichhardt and C. J. Olson Reichhardt, Phys. Rev. Lett. **92**, 108301 (2004).
[48] C. Reichhardt and C. J. Olson, Phys. Rev. Lett. **89**, 078301 (2002).
[49] See, e.g., R. F. Sekerka, J. Cryst. Growth **264**, 530 (2004), and references therein.
[50] D. M. Anderson, G. B. McFadden, and A. A. Wheeler, Physica D **2711**, 1 (2001).
[51] D. M. Anderson, G. B. McFadden, and A. A. Wheeler, in *Interfaces for the Twenty-First Century*, edited by M. K. Smith, M. J. Mixis, G. B. McFadden, G. P. Neitzel, and D. R. Canright (Imperial College Press, London, 2001), p. 131.
[52] R. Tönhardt and G. Amberg, Phys. Rev. E **62**, 828 (2000).